Title

Method for estimation of apoptotic cell fraction of cytotherapy using in vivo fluorine-19 magnetic resonance: pilot study in a patient with head and neck carcinoma receiving tumor-infiltrating lymphocytes labeled with perfluorocarbon nanoemulsion

Journal

Journal for ImmunoTherapy of Cancer, 11(6)

ISSN

2051-1426

Authors

Ahrens, Eric T

Helfer, Brooke M

O'Hanlon, Charles F

et al.

Publication Date

2023-06-01

DOI

10.1136/jitc-2023-007015

Peer reviewed

Journal for ImmunoTherapy of Cancer

Method for estimation of apoptotic cell fraction of cytotherapy using in vivo fluorine-19 magnetic resonance: pilot study in a patient with head and neck carcinoma receiving tumor-infiltrating lymphocytes labeled with perfluorocarbon nanoemulsion

Eric T Ahrens ,[1] Brooke M Helfer,[2] Charles F O'Hanlon,[3] Deanne R Lister,[1] Julie L Bykowski,[1] Karen Messer,[4] Benjamin I Leach,[1] Jiawen Chen,[5] Hongyan Xu,[1] Gregory A Daniels,[6] Ezra E W Cohen[6]

To cite: Ahrens ET, Helfer BM, O'Hanlon CF, *et al*. Method for estimation of apoptotic cell fraction of cytotherapy using in vivo fluorine-19 magnetic resonance: pilot study in a patient with head and neck carcinoma receiving tumor-infiltrating lymphocytes labeled with perfluorocarbon nanoemulsion. *Journal for ImmunoTherapy of Cancer* 2023;**10**:e007015. doi:10.1136/jitc-2023-007015

Accepted 21 May 2023

For numbered affiliations see end of article.

Correspondence to
Dr Eric T Ahrens;
eahrens@ucsd.edu

ABSTRACT

Background Adoptive transfer of T cells is a burgeoning cancer therapeutic approach. However, the fate of the cells, once transferred, is most often unknown. We describe the first clinical experience with a non-invasive biomarker to assay the apoptotic cell fraction (ACF) after cell therapy infusion, tested in the setting of head and neck squamous cell carcinoma (HNSCC). A patient with HNSCC received autologous tumor-infiltrating lymphocytes (TILs) labeled with a perfluorocarbon (PFC) nanoemulsion cell tracer. Nanoemulsion, released from apoptotic cells, clears through the reticuloendothelial system, particularly the Kupffer cells of the liver, and fluorine-19 (^{19}F) magnetic resonance spectroscopy (MRS) of the liver was used to non-invasively infer the ACF.

Methods Autologous TILs were isolated from a patient in their late 50s with relapsed, refractory human papillomavirus-mediated squamous cell carcinoma of the right tonsil, metastatic to the lung. A lung metastasis was resected for T cell harvest and expansion using a rapid expansion protocol. The expanded TILs were intracellularly labeled with PFC nanoemulsion tracer by coincubation in the final 24 hours of culture, followed by a wash step. At 22 days after intravenous infusion of TILs, quantitative single-voxel liver ^{19}F MRS was performed in vivo using a 3T MRI system. From these data, we model the apparent ACF of the initial cell inoculant.

Results We show that it is feasible to PFC-label ~70×10^{10} TILs (F-TILs) in a single batch in a clinical cell processing facility, while maintaining >90% cell viability and standard flow cytometry-based release criteria for phenotype and function. Based on quantitative in vivo ^{19}F MRS measurements in the liver, we estimate that ~30% cell equivalents of adoptively transferred F-TILs have become apoptotic by 22 days post-transfer.

Conclusions Survival of the primary cell therapy product is likely to vary per patient. A non-invasive assay of ACF over time could potentially provide insight into the mechanisms of response and non-response, informing future clinical studies. This information may be useful to developers of cytotherapies and clinicians as it opens an avenue to quantify cellular product survival and engraftment.

WHAT IS ALREADY KNOWN ON THIS TOPIC

⇒ Large numbers of cells (>10^9) are often infused in cytotherapies, but the viability of the transferred cell product over time is mostly unknown postdelivery.

WHAT THIS STUDY ADDS

⇒ We describe a fluorine-19 magnetic resonance spectroscopy method to non-invasively estimate the apoptotic cell fraction (ACF) after cell transfer.

⇒ In a proof-of-principle study, the method was applied to a patient with head and neck carcinoma receiving tumor-infiltrating lymphocyte therapy.

HOW THIS STUDY MIGHT AFFECT RESEARCH, PRACTICE OR POLICY

⇒ The ability to non-invasively assay cell graft survival may potentially explain responders versus non-responders and provide a tool for investigations into improving the cell product and its delivery, as well as conditioning protocols.

⇒ Future studies are needed to establish a potential correlation between ACF and patient outcomes.

BACKGROUND

Head and neck squamous cell carcinoma (HNSCC) is the sixth most common cancer worldwide, and within the USA it accounts for 3% of all cancers diagnosed annually and 2% of cancer-related deaths. Worldwide,

there were 890 000 new cases and 450 000 deaths related to HNSCC in 2018. The incidence of HNSCC continues to rise and is anticipated to increase by 30% by 2030 (Global Cancer Observatory). The rapid rise in HNSCC is primarily due to increases in human papillomavirus (HPV)-associated oropharynx cancers. Most patients with HNSCC initially present with advanced stage disease (stage III–IV).[1] Despite aggressive, combined modality treatment, a significant proportion of patients will develop locoregionally recurrent or metastatic disease that is no longer amenable to curative therapy. Cancer immune therapy has transformed oncology practice with multiple agents, ranging from vaccines, cytokines, and checkpoint inhibitors, to cell products. The effectiveness of the immune system to selectively target 'rare events' allows immunotherapy to synergistically supplement surgery, chemotherapy, and radiotherapy. Anti-programmed cell death protein 1 (PD1) antibodies represent a standard of care for patients with HNSCC, but response rates and survival outcomes remain poor[1]; thus, there is an urgent need to improve therapeutic strategies.

The tumor microenvironment (TME) offers a window to predict patient outcomes as well as a source of effector cells. Tumors rich in lymphocytic infiltration have a better prognosis. In fact, patients can be risk-stratified based on an 'immunoscore' that outperforms tumor, node, and metastasis staging in patients with colorectal cancer[2] and other solid tumors.[3] The immune cells in the TME are not only prognostic and predictive of outcomes and therapy response but can be used as a therapeutic tool. Using ex vivo manipulation of tumor-infiltrating lymphocytes (TILs), early work by Rosenberg *et al*[4] demonstrated the therapeutic benefits of TILs when given to patients. TIL infusions can yield durable responses in a variety of patients with solid tumor, including but not limited to patients with melanoma, cervical cancer, and head and neck cancer.[5] The National Cancer Institute demonstrated in three consecutive trials the successful treatment of metastatic melanoma with adoptive transfer of TILs in patients who received autologous product following a lymphodepleting regimen plus interleukin-2 (IL-2) administration, with or without total body irradiation.[6] The overall objective response rate using the RECIST (Response Evaluation Criteria in Solid Tumors) criteria in 93 patients was 56%. Thus, TIL therapy demonstrated immune-mediated regression in a significant fraction of patients with refractory metastatic melanoma. The National Cancer Institute and others have expanded the use of the same TIL product to other solid tumors, including HPV-associated malignancies and gastrointestinal tumors.[7] Cell product has been successfully manufactured and delivered in an analogous manner to patients with HPV-associated HNSCC at the University of California San Diego. The application of TILs may expand as we understand better the regulatory control and nature of the effector response.

Despite observable tumor responses to adoptive transfer, the mechanism of action remains opaque as there are few non-invasive methods for detecting the fate of a lymphocyte product post-transfer, beyond what is detectable in blood samples or from invasive bone marrow aspirates. In these cell therapies, very large numbers of cells (>1 billion) are often infused. The fate and biodistribution of cells may be predictive of therapeutic outcomes; however, the viability of the transferred cell product over time is currently unknown in most settings, particularly when cell product phenotype is indistinguishable from endogenous cells. The ability to non-invasively assay cell survival (or apoptosis) in real time, which is likely to vary from patient to patient, may potentially explain responders versus non-responders, allow for early assessment of non-response, and support investigation of improved delivery and conditioning protocols to better inform a personalized cell delivery approach.

To address the question of cell product viability postinfusion, we describe a novel non-invasive biomarker to estimate the apoptotic cell fraction (ACF) after adoptive T cell transfer. The biomarker employs a perfluorocarbon (PFC) nanoemulsion cell tag, combined with fluorine-19 (^{19}F) magnetic resonance spectroscopy (MRS) detection. This method was evaluated in a patient with recurrent HNSCC receiving autologous TIL infusion at the University of California San Diego. During the final growth phase, the entire culture (>10 billion TILs) was intracellularly labeled in a clinical cell processing laboratory with PFC nanoemulsion by an overnight coincubation. Following wash and quality control release steps, the labeled product (F-TIL) was infused into the patient. Post-transfer, cell apoptosis was monitored by detecting the presence of the ^{19}F tag in the liver using quantitative ^{19}F MRS; apoptotic F-TILs release the nanoemulsion droplets, which are phagocytosed by cells of the reticuloendothelial system (RES) and accumulate predominantly in the Kupffer cells of the liver. Overall, we show that it is possible to estimate the ACF using PFC cellular labels and ^{19}F MRS. These methods are broadly applicable to a wide range of cell types and clinical trials.

METHODS

Patient profile

The patient was in their 50s with relapsed, refractory HPV-mediated squamous cell carcinoma of the right tonsil, metastatic to the lung. The original diagnosis was 4 years prior, and treatment had included primary surgery and adjuvant radiation therapy. Recurrence within 2 years was treated with carboplatin/paclitaxel/cetuximab, and the patient was subsequently treated with pembrolizumab on clinical trials and docetaxel/cisplatin. A 3 cm right middle lobe metastasis was resected for cell harvest. CT of the chest, abdomen and pelvis, and brain, as well as ^{1}H MRI were performed 13 days prior to TIL infusion, confirming persistent bilateral pulmonary metastases and right pleural effusion. No liver or central nervous system metastases were evident on this clinical scan.

Preparation of F-TILs

The patient's tumor was surgically resected and transferred to the Advanced Cell Therapy Laboratory at the University of California San Diego Medical Center. The resected tumor was processed within 24 hours postisolation. The tumor was cut into small fragments, and individual fragments were cultured with IL-2 (Prometheus, 6000 IU/mL) containing RPMI (Roswell Park Memorial Institute, Gibco) media in multiwell plates. TILs present in the tumor fragments were allowed to proliferate; on reaching a cell count of ~8×10^6 per well, cells were cryopreserved prior to entering the rapid expansion phase of TIL production. For the rapid expansion protocol, TILs were cultured with irradiated peripheral blood mononuclear cells as feeder cells. Over a 14-day period, the cells were expanded in RPMI and AIM V Media (Gibco) supplemented with 5% human AB serum and 6000 IU/mL of IL-2. TILs were intracellularly PFC-labeled at the final growth phase to yield F-TIL product. On day 13, PFC nanoemulsion (CS-1000, Celsense) was added to the TIL culture at 10 mg/mL for the final 24 hours of expansion, followed by a wash step on day 14, and the F-TILs were harvested and packaged into sterile infusion bags.

Release criteria for F-TILs

The acceptance criteria for F-TIL included a viability assay, trypan blue exclusion, measured via TC20 Automated Cell Counter (BioRad). The acceptance is set at not less than (NLT) 70% viable. Also, cell density and cell count were determined from this measurement with an accepted cell count of NLT 1×10^9 cells. The F-TIL identity and potency were established from an interferon gamma (IFNɣ) release assay. IFNɣ+ T cells were assayed by intracellular staining with and without soluble CD3 (OKT3, Miltenyi Biotec) stimulation. Briefly, after control or OKT3 stimulation with Golgi Plug and Golgi Stop (Miltenyi Biotec), cells were pelleted and stained with Viobility 405/520 (Miltenyi Biotec), followed by CD3-VioBlue, CD4-FITC, and CD8-PE (all from Miltenyi Biotec). Lastly, cells were treated with Inside Stain (Miltenyi Biotec) and then stained with anti-IFNγ-APC (Miltenyi Biotec). Cellular preparations were assayed using a Miltenyi MACSQuant 10 analyzer.

^{19}F nuclear magnetic resonance assay of F-TIL labeling

To assay the mean ^{19}F/cell of the F-TIL product, we performed ^{19}F nuclear magnetic resonance (NMR) spectroscopy of F-TIL pellets. Pellets with 3 million cells (n=3) were treated with 100 µL of lysis buffer (200 mM Tris, 100 mM NaCl, 1 mM EDTA, and 0.5% Triton). Subsequently, 100 µL 0.1% trifluoroacetic acid (TFA, dH_2O/D_2O, 9:1 v/v, 2.43×10^{18} total F-atoms) was added as reference. Samples were placed in a 5 mm NMR tube, and ^{19}F spectra were acquired using a 400 MHz spectrometer (NanoBay, Bruker BioSpin). A single pulse sequence (Bruker) was used with 16 averages, repetition time (TR) of 15 s, 65 536 real spectral points, and sweep width of 37 500 Hz. Spectra for PFC (−92 ppm) and TFA (−76 ppm) were fitted and integrated. The mean ^{19}F/cell ($\bar{F}_c$) was calculated using the following equation:

$$\bar{F}_c = \frac{3I_s M_r N_a}{I_r N_c} \quad (1)$$

where I_s=integrated area of PFC peak, M_r=moles of TFA reference (three ^{19}F per TFA), N_a=Avogadro's number, I_r=integrated area of TFA peak, and N_c=number of cells in the pellet.

Clinical ^{19}F magnetic resonance

Post-transfer, liver ^{19}F MRS was performed using a GE Discovery MR750 3T imaging system equipped with vendor-supplied multinuclear spectroscopy package and an aftermarket ^{19}F transmit-receive surface coil (33×24 cm; RAPID Biomedical). As the gyromagnetic ratio of ^{19}F is close to ^{1}H (~0.94 quotient), the same coil element can be used (non-optimally) for ^{1}H imaging. A TFA reference standard (6.08×10^{20} total F-atoms, 250 µL 10% TFA+250 µL 2% agarose in 10 mm diameter glass tube, 1.5 cm length) was affixed to the patient's side of the surface coil housing for absolute F-quantification. The surface coil was placed directly over the liver along the lower ribs and right upper quadrant of the abdomen and secured with straps that allowed for respiratory motion. A ^{1}H gradient echo localizer with TR of 4.7 ms, echo time (TE) of 1.3 ms, 256×128 matrix, 48 cm inplane field of view, slice thickness of 10 mm, and with 10 slices was used to identify the anatomy in three orthogonal planes for placement of liver and TFA reference voxels for serial MRS acquisitions. ^{19}F MRS was performed using a PRESS sequence (point resolved spatially localized spectroscopy), with the following parameters: TR/TE=1000/30 ms, spectral width=5000 Hz, number of points=2048, and voxel sizes of 15.6 cm^3 (2.5×2.5×2.5 cm^3) for the liver and 8 cm^3 (2×2×2 cm^3) for TFA reference. The TFA voxel encompassed the entire reference tube. The averages were 256 and 128, with total acquisition times of 4.4 min and 2.2 min for the liver and TFA, respectively. The PFC has a ^{19}F longitudinal relaxation time of T_1=0.47 s at 3T.

^{19}F/^{1}H phantom

An MRI phantom was prepared using a 4 L plastic container filled with 1% agarose with 20 mM NaCl. The surface coil was placed on phantom, and a ^{1}H gradient echo localizer pulse sequence was used for imaging, as above. In central axial slice, a radial array of region of interest (ROI) integrated intensity values was measured. The plot of intensity drop-off with radial distance was spline-fit and used to estimate signal drop-off at the liver voxel centroid location. Both ^{1}H and ^{19}F use the same radiofrequency (RF) coil and thus the RF homogeneity profile for the two nuclei is assumed to be equivalent.

Computed tomography

The total liver volume was segmented from the pretreatment, contrast-enhanced clinical CT scan using VivoQuant V.4.0 software (Invicro), excluding the hepatic veins and portal veins and their proximal branches.

MRS signal processing

Fourier transform and phase correction of the ^{19}F MRS data were implemented using the MATLAB software (V.R2019a; MathWorks), with a 20 Hz Gaussian window function applied. The resulting spectra were fit to a Lorentzian function using the Origin software (OriginLab) to extract the baseline, integrate the signals, and calculate fit uncertainty.

Murine PFC biodistribution

The biodistribution of PFC nanoemulsion following systemic delivery was evaluated in a mouse. Wild-type C57BJ/6 mice (Jackson Laboratories), 8–10 weeks old, were injected via the tail vein with PFC nanoemulsion (0.2 mL 30% v/v, 1.2×10^{21} F-atoms, blood half-life ~10 hours). Data were acquired in intact, necropsied tissue/organ panels at days 7 (n=4), 14 (n=5), or 21 (n=5) postadministration. PFC biodistribution was assayed in whole-organ panels using quantitative ^{19}F NMR spectroscopy; detailed methods are described elsewhere.[8]

Estimation of ACF

The ACF of the cell graft in vivo is calculated from the following:

$$ACF = \alpha^{-1}\left(\frac{N_L}{N_i}\right) \quad (2)$$

where α=liver partition fraction, that is, the fraction of PFC nanoemulsion mass in biodistribution residing in the liver after blood clearance and RES uptake; N_i=total number of F-labeled cells injected; and N_L=the total F-labeled cell equivalents in the liver tissue.

Specifically, using ^{19}F MRS, we measure N_L in the subject using the relationship:

$$N_L = \bar{F}_c^{-1}\left(\frac{I_v F_{TFA}}{I_{TFA}}\right)\left(\frac{V_L}{V_v}\right)\beta\delta \quad (3)$$

where $\bar{F}_c$=mean ^{19}F per cell after labeling measured in cell pellet by NMR spectroscopy (equation 1), I_v=integrated intensity of ^{19}F PFC peak normalized to average number, I_{TFA}=integrated intensity of ^{19}F TFA peak normalized to averages, F_{TFA}=total F-content of TFA reference (6.08×10^{20} F-atoms), V_L=segmented volume of the liver measured from CT scan, V_v=volume of ^{19}F PRESS voxel of the liver, and β=fractional correction for intensity drop-off at the location of spectroscopy voxel due to surface coil RF receptive field profile inhomogeneity. Note that if a homogenous RF volume coil is used, β ~1. Also, equation 3 considers the scenario where only a single repetition time (TR) of the pulse sequence is used for both PFC and TFA acquisitions, where full spin magnetization recovery of TFA does not occur due to its longer T_1 compared with PFC; in this case $\delta\neq1$, and this correction can be expressed as the following:

$$\delta = \left(1 - e^{\frac{-TR}{T_1^{TFA}}}\right) / \left(1 - e^{\frac{-TR}{T_1^{PFC}}}\right) \quad (4)$$

Table 1 Summary of fluorine-labeled tumor infiltrating lymphocyte (F-TIL) product characteristics on release

F-TIL properties	
Final product volume	690 mL
Total viable cells (N_i)	7×10^{10}
Viability	91.3%
Concentration	1.08×10^{8} viable cells/mL
Gram stain	No growth
Endotoxin level	1.47 EU/kg
Rapid mycoplasma detection	Negative
Frequency of IFNγ+ CD3+ T cells	36.67%
Ratio of IFNγ+ T cells vs control IFNγ+ T cells*	137
Mean† ^{19}F/cell ($\bar{F}_c$)	$1.77\times10^{11}\pm0.04$

*The control is non-OKT3-stimulated F-TIL.
†Not part of product release criteria.
F-TIL, fluorine-labeled tumor infiltrating lymphocyte; IFNγ, interferon gamma.

RESULTS

F-TIL product characterization

During the last 24 hours of TIL expansion, the cells were labeled with PFC nanoemulsion by coincubation, followed by a wash step. F-TILs were condensed and pooled for patient formulation into two infusion bags, with additional product

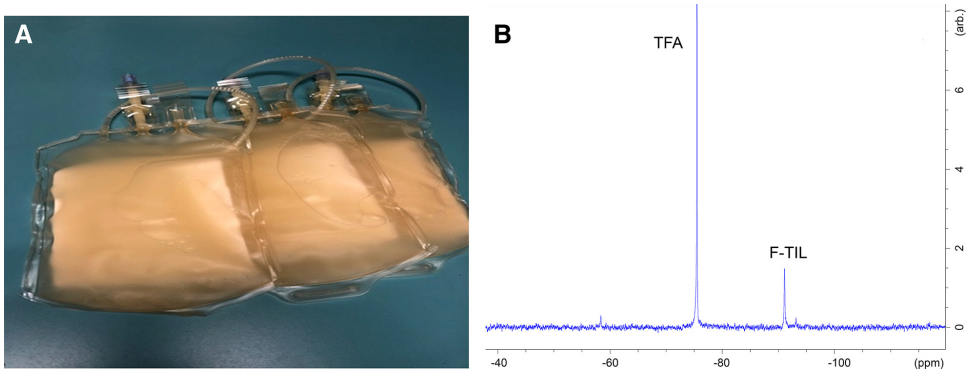

Figure 1 Labeled F-TIL product. (A) The final batch of 70×10^9 F-TIL cells. (B) Representative (n=3) ^{19}F NMR spectrum of a pellet of F-TIL (–92 ppm) and TFA reference (–76 ppm) peaks. The NMR sample contained 3×10^6 F-TIL, 100 µL TFA, and 9:1 H_2O/D_2O. ^{19}F NMR, fluorine-19 nuclear magnetic resonance; F-TIL, fluorine-labeled tumor infiltrating lymphocyte; TFA, trifluoroacetic acid.

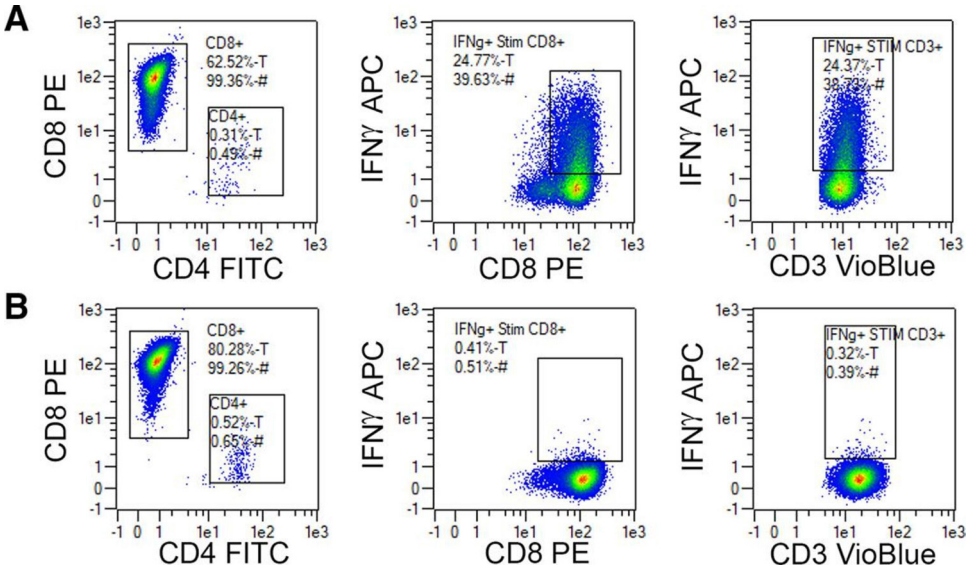

Figure 2 Flow cytometry phenotypic analysis of F-TIL±OKT3 stimulation. (A) Stimulated/stained and (B) unstimulated/stained. The gating strategy applied to the panels was lymphocytes → live cells → CD3+. Controls include blank, stimulation/unstained, and unstimulated/unstained samples (not shown). Overall, the data show that stimulated CD3 F-TIL meets the specification of >3% IFNγ-producing cells, where levels of IFNγ are greater than the stained unstimulated control. F-TIL, fluorine-labeled tumor infiltrating lymphocyte; INFγ, interferon gamma.

set aside for release testing. Figure 1A displays a photograph of the final batch (690 mL), where 230 mL aliquots are packaged into infusion bags. Table 1 summarizes the properties of the F-TIL product. Cellular viability postexpansion was 91.3%. F-TILs were prepared at 1.08×10^8 viable cells per milliliter, for a total of 7×10^{10} cells.

The total fluorine content was also assessed on a sample of the pooled cells. Figure 1B displays a representative ^{19}F NMR spectrum of an F-TIL pellet (3×10^6 cells). From the integrated areas under the PFC and TFA peaks, the mean ^{19}F/cell per cell ($\bar{F}_c$) was calculated to be $1.77\times10^{11}\pm0.04$ ^{19}F/cell (n=3) using equation 1.

The F-TIL phenotype±OKT3 stimulation was also assayed using flow cytometry (figure 2). Overall, the data show that stimulated F-TIL has levels of IFNγ that are greater than the stained, unstimulated control (figure 2), and the product met the release specification of >3% IFNγ-producing cells.

^{19}F MRS and estimation of ACF

The patient was clinically stable prior to receiving the TIL infusion and no reaction was noted on receiving the dose. The patient was scanned using ^{19}F MRS on day 22 after F-TIL infusion. The surface coil used for the experiment is displayed in figure 3A. Localizing ^{1}H MRI scans confirming placement over the liver are displayed in figure 3B, which also shows the positioning of the localized PRESS voxels for PFC and TFA ^{19}F MRS. Figure 3C shows the PRESS ^{19}F spectra for PFC (liver) and TFA. We note that the patient's largest metastasis was proximal to the aorta, and due to large vasomotion ^{19}F MRS was not attempted at this site.

Using the ^{19}F MRS data and equation 2, the ACF was estimated to be 30%, or alternatively (1–ACF)×100=70% 'cell-equivalent' viable cells. This calculation uses the number of viable injected cells (N_i; table 1), N_L (equation 3), and the total cell number equivalents in the liver measured via single-voxel ^{19}F MRS. An additional parameter used for ACF (equation 2) is the 'liver partition fraction' (α), which is the fraction of PFC nanoemulsion mass in the liver following uptake into the RES. We estimate the magnitude of α ~0.83, based on the average of the empirical values calculated at days 7, 14, and 21 postadministration using murine PFC biodistribution data as a model (figure 4). The ACF does not consider potential

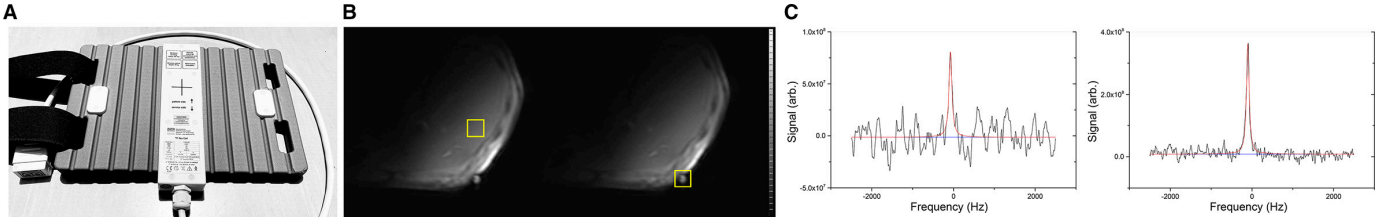

Figure 3 Patient liver ^{19}F MRS. (A) ^{19}F surface coil used. (B) An axial ^{1}H MRI slice of the subject's liver and single-voxel placements (yellow) in the liver (left) and TFA reference (right) for ^{19}F MRS. (C) ^{19}F spectra of the liver (left) and TFA (right), where solid lines are fits. ^{19}F MRS, fluorine-19 magnetic resonance spectroscopy; TFA, trifluoroacetic acid.

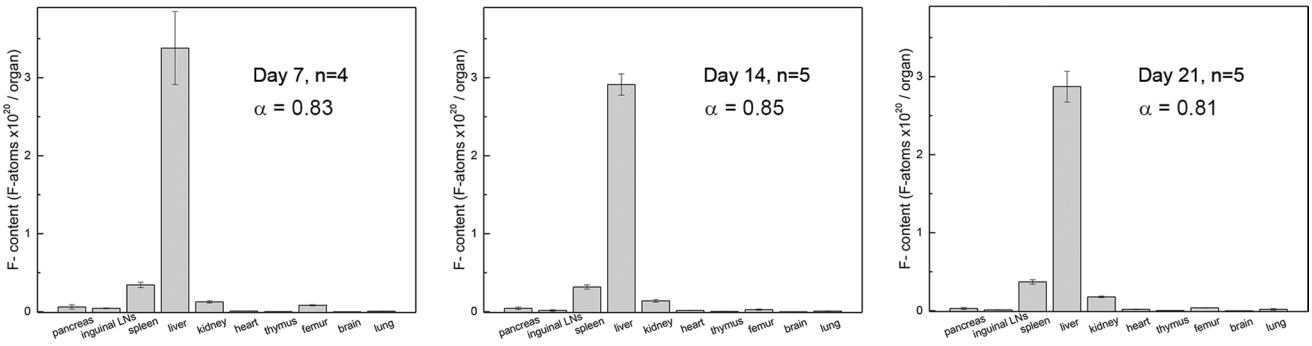

Figure 4 PFC nanoemulsion biodistribution following systemic delivery in a mouse. Wild-type C57BJ/6 mice were used to estimate relative PFC nanoemulsion biodistribution in the liver (α). Data were acquired in intact, necropsied tissues/organs at 7, 14, and 21 days after intravenous delivery of PFC nanoemulsion using quantitative ^{19}F NMR spectroscopy.[8] The biodistribution displays the expected RES uptake, dominated by liver uptake of PFC, and PFC persistence for >21 days. ^{19}F NMR, fluorine-19 nuclear magnetic resonance; LN, lymph node; PFC, perfluorocarbon; RES, reticuloendothelial system.

cell division in vivo, which would approximately equally divide the ^{19}F tracer between daughter cells.

In the calculation of N_L (equation 3), we use the total liver parenchymal volume (V_L), estimated via manual segmentation of the contrast-enhanced CT scan (figure 5) performed prior to F-TIL infusion. In this segmentation, the hepatic veins, portal veins, and their proximal branches were excluded from the volume measurement. Overall, the volume was found to be 1862±93 cm^3.

In equation 3, we also use a ^{1}H MRI phantom experiment to empirically estimate the RF receptive field drop-off correction (β parameter; equation 3) at the liver voxel location due to surface coil utilization.[9] The ^{1}H MRI intensity profile in phantom is shown in figure 6A, along with the ROI intensity values along a radial from surface coil (figure 6B). The red asterisk in figure 6B indicates the approximate centroid location of the liver voxel used in the patient scan, where the signal falloff is ~13.5% and thus β ~1.135. Additionally, we estimate δ ~0.45, which is a correction for the incomplete recovery of the TFA ^{19}F longitudinal magnetization due to the short TR (1000 ms).

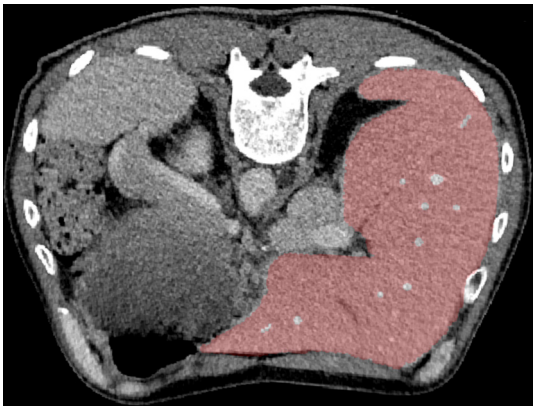

Figure 5 CT segmentation of the liver. Shown is a representative axial CT slice of the liver with segmentation mask overlaid (magenta).

DISCUSSION/CONCLUSIONS

In a first-in-human pilot study, we describe a novel non-invasive method to estimate the in vivo survival of an intravenously delivered cell therapy product, tested in a patient with HNSCC receiving F-TIL therapy. The ACF metric represents the inferred number of transferred cells that have died, referenced to the initial cell dose. This approach has the advantage of being based on a straightforward quantitative, single-voxel MRS measurement of ^{19}F-spin number in the liver, which is the dominant clearance organ for tracer released by apoptotic cells. Given the promising results so far with different cell therapies in tumors, both liquid and solid, a non-invasive method to assess graft survival would be of value. Longitudinal assessments would allow correlation of ACF with efficacy and would inform development strategies to enhance product survival and transmission to tumor. Moreover, the dynamics of survival of the transferred cells over time may provide an early marker of response or non-response. Importantly, we show that it is feasible to ^{19}F-tag large batches of autologous T cells (~70×10^{10}) in a good manufacturing practice cell processing lab, while maintaining viability and conventional cell product release criteria.

The in vivo fate of cell-released tracer has been studied extensively in murine models. Early work[10] first reported a prominent ^{19}F liver signal following intravenous injection of PFC-labeled dendritic cells (DCs), which was associated with tracer uptake after release from dead cells. Subsequent studies of the biodistribution of chimeric antigen receptor (CAR) T cells in a solid tumor model in mice reported[11] liver ^{19}F signals that gradually increased over time, corresponding to approximately 15% and 30% of initially injected cell equivalents by day 2 and 14 postgraft, respectively. In these mice, colocalization of PFC nanoemulsion and Kupffer cells of the liver was validated by immunohistochemistry, where CAR T cells were labeled with a 'dual-mode' PFC nanoemulsion having a fluorescent tag conjugated to the nanoemulsion, thereby enabling endpoint tracer detection in immunostained

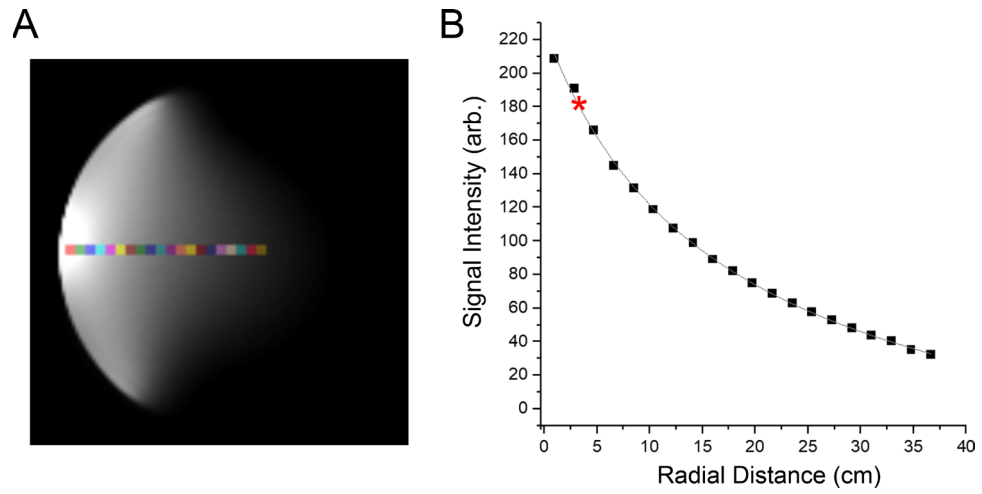

Figure 6 Phantom studies. The ^{1}H MRI intensity profile in agar phantom is shown (A), along with ROI intensity values along a radial from surface coil (B). The red asterisk indicates the approximate centroid location of the liver voxel used in the patient scan (figure 3B). ROI, region of interest.

(F4/80) liver sections. Moreover, Rose *et al*[12] report that in labeled stem cells, on induction of cell death, >95% of ^{19}F was released from cells, indicating that fluorine retention can be used as a surrogate marker of cell survival. Also, we note that there is no evidence of tracer leakage or exocytosis of PFC nanoemulsion in viable labeled cells, or by cells undergoing mitosis, for example, as demonstrated in live-cell, time-lapse confocal microscopy studies using dual-mode nanoemulsion.[13]

There are several assumptions made in our ACF model (equation 2). The N_L calculation assumes that the distribution of PFC in the liver, which is harbored in the Kupffer cells, is homogenous over the liver parenchymal volume. The patient did not have liver metastases; however, metastatic involvement or other benign liver lesions could confound this assumption. The patient was imaged at 22 days postinfusion, allowing for recovery and discharge from the hospital. As the clearance of the PFC from the body is slow (>250 days), we assume that agent clearance is insignificant compared with the time scale of our measurement at 22 days. For long-term longitudinal studies, the model in equation 2 could be modified to include a term correcting for gradual PFC clearance and subsequent ^{19}F signal decrease. We note that the intact PFC molecule ultimately clears the body, without chemical modification in vivo, via lung exhalation.[14] The clearance rate depends strongly on the PFC molecular structure,[15] for example, perfluoropolyether (CS-1000) and perfluorooctyl bromide have half-lives of >250 and ~12 days, respectively. Additionally, the ACF model does not consider cell proliferation of transferred cells, as the reference point for ACF is the initial injected dose. TILs can display a propensity for proliferation in vivo. On cell division, the PFC tracer is partitioned and diluted approximately equally between daughter cells.[16] Thus, the model could lead to underestimation at the measurement time point, for example, if only one of the daughter cells has undergone apoptosis; thus, the inferred ACF fraction is a lower bound. The largest source of uncertainty in the ACF calculation is estimation of partition fraction, α, which was estimated from mouse. However, species-specific uncertainty in this parameter will likely only affect the accuracy by a moderate amount and represents a constant, systematic error, which would not affect reproducibility of the assay. Refinement of the α parameter could be obtained using comparable PFC biodistributions studies in non-human primates, for example.

The CS-1000 is a first-generation PFC nanoemulsion imaging agent designed for ex vivo cell labeling of cell therapy prior to patient graft. In prior studies, CS-1000 was used in a phase I clinical trial for late-stage colorectal cancer treatment with a DC vaccine, where ^{19}F MRI was used to visualize and quantify labeled DCs postadministration.[17] This study is the first clinical use of CS-1000 for a T lymphocyte product. CS-1000 has also been broadly applied in non-clinical studies to image a wide range of cell types, including various stem and progenitor cells,[18–23] DCs,[10 17 24] T cells,[11 16 25–27] and natural killer cells.[28 29]

Overall, the use of immunotherapeutic lymphocyte cell products, particularly engineered T cells, has received a huge investment over the past few years and has made transformative inroads toward 'curative' clinical outcomes for certain cancers. Currently, there is a lack of non-invasive measurement tools for detecting the fate of the transferred cells after they leave the bloodstream. In this study, we describe a ^{19}F-based biomarker method to estimate ACF after cell infusion. This technology opens the door to enhanced monitoring in the setting of any type of adoptive cell therapy. This information may be useful for cell product developers and clinicians by providing insight into the fate of the cellular product once it enters the patient. However, future studies are needed to establish a correlation between ACF and patient outcomes and to validate the predictive ability of the ACF metric.

Author affiliations
[1]Department of Radiology, University of California San Diego, La Jolla, California, USA
[2]Celsense, Pittsburgh, Pennsylvania, USA
[3]Lot 49 Consulting, Pittsburgh, Pennsylvania, USA
[4]Division of Biostatistics, University of California San Diego, La Jolla, California, USA
[5]Department of Electrical and Computer Engineering, University of California San Diego, La Jolla, California, USA
[6]Department of Medicine, University of California San Diego, La Jolla, California, USA

Acknowledgements We acknowledge Dr Rolf Schulte, General Electric, for valuable MRI/MRS pulse sequence assistance.

Contributors ETA conceived the methods and helped with trial design, analyzed the data, wrote the final draft, and study guarantor. BMH formulated the PFC nanoemulsion, designed the cell labeling protocol, performed preliminary in vitro cell testing, and assisted with IND and manuscript write-ups. CFO'H assisted with PFC nanoemulsion formulation and regulatory filings. DRL performed MRI/MRS data acquisitions, data analysis, and writing. JLB performed anatomical analysis of patient data and assisted with patient data acquisitions and study write-up. KM performed statistical analysis and manuscript editing. BIL performed NMR and MRS data analyses and study write-up. JC performed MRS data analysis. HX prepared MRI/MRS phantoms and assisted with study management and data analysis. GAD provided patient selection and care and aided in regulatory filings. EEWC assisted with study design, patient selection, patient care, study management, and manuscript preparation.

Funding Funding was provided by the National Institutes of Health (NIH) (grant R01-CA134633).

Competing interests None declared.

Patient consent for publication Not required.

Ethics approval This study involves human participants and was approved by UC San Diego's Institutional Review Board (IRB #160710) and by the US Food and Drug Administration (FDA) as an investigative new drug (IND #18932). The PFC nanoemulsion imaging agent (CS-1000, Celsense) is the subject of US FDA Drug Master File (#BB-MF14062), which contains detailed chemistry, manufacturing, and control information, stability studies, results of various cytotoxicity and phenotype studies in numerous cell types (including human T cells), and results of rodent acute toxicity studies and genotoxicity studies. All animal experiments followed a protocol (#S12237) approved by the University's Institutional Animal Care and Use Committee. Participants gave informed consent to participate in the study before taking part.

Provenance and peer review Not commissioned; externally peer reviewed.

Data availability statement Data are available upon reasonable request.

ORCID iD
Eric T Ahrens http://orcid.org/0000-0001-6131-9304

REFERENCES

1 Sacco AG, Cohen EE. Current treatment options for recurrent or metastatic head and neck squamous cell carcinoma. *J Clin Oncol* 2015;33:3305–13.
2 Galon J, Mlecnik B, Bindea G, *et al*. Towards the introduction of the 'Immunoscore' in the classification of malignant tumours. *J Pathol* 2014;232:199–209.
3 Donnem T, Hald SM, Paulsen E-E, *et al*. Stromal Cd8(+) T-cell density-a promising supplement to TNM staging in non-small cell lung cancer. *Clin Cancer Res* 2015;21:2635–43.
4 Rosenberg SA, Packard BS, Aebersold PM, *et al*. Use of tumor-infiltrating lymphocytes and Interleukin-2 in the immunotherapy of patients with metastatic Melanoma. *N Engl J Med* 1988;319:1676–80.
5 Radvanyi LG. Tumor-infiltrating lymphocyte therapy: addressing prevailing questions. *Cancer J* 2015;21:450–64.
6 Dudley ME, Gross CA, Somerville RPT, *et al*. Randomized selection design trial evaluating CD8(+)-enriched versus unselected tumor-infiltrating lymphocytes for adoptive cell therapy for patients with melanoma. *J Clin Oncol* 2013;31:2152–9.
7 Stevanović S, Draper LM, Langhan MM, *et al*. Complete regression of metastatic cervical cancer after treatment with human papillomavirus-targeted tumor-infiltrating T cells. *J Clin Oncol* 2015;33:1543–50.
8 Ahrens ET, Young W-B, Xu H, *et al*. Rapid quantification of inflammation in tissue samples using perfluorocarbon emulsion and fluorine-19 nuclear magnetic resonance. *Biotechniques* 2011;50:229–34.
9 Axel L, Costantini J, Listerud J. Intensity correction in surface-coil MR imaging. *AJR Am J Roentgenol* 1987;148:418–20.
10 Ahrens ET, Flores R, Xu H, *et al*. In vivo imaging platform for tracking immunotherapeutic cells. *Nat Biotechnol* 2005;23:983–7.
11 Chapelin F, Gao S, Okada H, *et al*. Fluorine-19 nuclear magnetic resonance of chimeric antigen receptor T cell biodistribution in murine cancer model. *Sci Rep* 2017;7:17748.
12 Rose LC, Kadayakkara DK, Wang G, *et al*. Fluorine-19 labeling of stromal vascular fraction cells for clinical imaging applications. *Stem Cells Transl Med* 2015;4:1472–81.
13 Patrick MJ, Janjic JM, Teng H, *et al*. Intracellular pH measurements using perfluorocarbon nanoemulsions. *J Am Chem Soc* 2013;135:18445–57.
14 Spahn DR. Blood substitutes. artificial oxygen carriers: perfluorocarbon emulsions. *Crit Care* 1999;3:R93–7.
15 Jacoby C, Temme S, Mayenfels F, *et al*. Probing different perfluorocarbons for in vivo inflammation imaging by 19F MRI: image reconstruction, biological half-lives and sensitivity. *NMR Biomed* 2014;27:261–71.
16 Srinivas M, Turner MS, Janjic JM, *et al*. In vivo cytometry of antigen-specific t cells using 19F MRI. *Magn Reson Med* 2009;62:747–53.
17 Ahrens ET, Helfer BM, O'Hanlon CF, *et al*. Clinical cell therapy imaging using a perfluorocarbon tracer and Fluorine-19 MRI. *Magn Reson Med* 2014;72:1696–701.
18 Boehm-Sturm P, Mengler L, Wecker S, *et al*. In vivo tracking of human neural stem cells with F-19 magnetic resonance imaging. *PLoS One* 2011;6:e29040.
19 Boehm-Sturm P, Mengler L, Wecker S, *et al*. In vivo tracking of human neural stem cells with 19F magnetic resonance imaging. *PLoS ONE* 2011;6:e29040.
20 Hoehn M, Küstermann E, Blunk J, *et al*. Monitoring of implanted stem cell migration in vivo: a highly resolved in vivo magnetic resonance imaging investigation of experimental stroke in rat. *Proc Natl Acad Sci U S A* 2002;99:16267–72.
21 Bible E, Dell'Acqua F, Solanky B, *et al*. Non-invasive imaging of transplanted human neural stem cells and ECM scaffold remodeling in the stroke-damaged rat brain by (19)F- and diffusion-MRI. *Biomaterials* 2012;33:2858–71.
22 Gaudet JM, Ribot EJ, Chen Y, *et al*. Tracking the fate of stem cell implants with fluorine-19 MRI. *PLoS One* 2015;10:e0118544.
23 Ribot EJ, Gaudet JM, Chen Y, *et al*. In vivo MR detection of fluorine-labeled human MSC using the bSSFP sequence. *Int J Nanomedicine* 2014;9:1731–9.
24 Helfer BM, Balducci A, Nelson AD, *et al*. Functional assessment of human dendritic cells labeled for in vivo (19)F magnetic resonance imaging cell tracking. *Cytotherapy* 2010;12:238–50.
25 Srinivas M, Morel PA, Ernst LA, *et al*. Fluorine-19 MRI for visualization and quantification of cell migration in a diabetes model. *Magn Reson Med* 2007;58:725–34.
26 Janjic JM, Srinivas M, Kadayakkara DKK, *et al*. Self-delivering nanoemulsions for dual fluorine-19 MRI and fluorescence detection. *J Am Chem Soc* 2008;130:2832–41.
27 Kadayakkara DK, Beatty PL, Turner MS, *et al*. Inflammation driven by overexpression of the Hypoglycosylated abnormal Mucin 1 (MUC1) links inflammatory bowel disease and Pancreatitis. *Pancreas* 2010;39:510–5.
28 Somanchi SS, Kennis BA, Gopalakrishnan V, *et al*. In vivo (19) F-magnetic resonance imaging of adoptively transferred NK cells. *Methods Mol Biol* 2016;1441:317–32.
29 Bouchlaka MN, Ludwig KD, Gordon JW, *et al*. (19)F-MRI for monitoring human NK cells in vivo. *Oncoimmunology* 2016;5:e1143996.